Silicon-substituted hydroxyapatite nanocomposite: Synthesis, characterization and in vitro bioactivity study in Human Serum Albumin

M. H. Loghmani[1]*, A. Abouzarzadeh[2]

[1]*Assistant Professor, Department of Nanotechnology, University of Guilan, Rasht, Iran*
[2]*MSc Student,Nanotechnology Research Institute, Babol University of Technology, Babol, Iran*
* Corresponding author's E-mail: mhmdloghmani@guilan.ac.ir

ABSTRACT
Nano hydroxyapatite and Silicon-substituted hydroxyapatite nanocomposites with various amount of Si contents (0, 2, 4 and 6 mole % as named as HS0, HS2, HS4 and HS6) were prepared via in situ hybridization method and were analyzed by XRD, FTIR, SEM and AFM techniques. Size distribution of the products demonstrated that hydroxyapatite particles size was between 2 and 53.5 nm with further mean size about 23 nm, while these results, were found to be present around 45, 32 and 38 nm for HS2, HS4 and HS6 respectively. The XRD results specified that some change occurred in the hydroxyapatite lattice with varying Si content in composites samples and explained incorporation of silicon did not appear significantly affect upon the diffraction pattern. SEM micrograph indicated many small particle crystallites existed in the aggregated surface that improved surface modification of composite products that might be due to the high solubility of the nanoparticles in the organic solvents. Subsequently soaking in Human Serum Albumin caused tiny particles observation in a new formation, as the new form of apatite layer covered the samples. In addition, it is quite obvious that the all peaks in FTIR remained after immersion, while peaks intensity was decreased.

Keywords: Hydroxyapatite; Silicon; Nanocomposites; Human Serum Albumin; Bioactivity

1. INTRODUCTION

In recent years, the development of bioactive composites commonly identified as bioanalogue have gained a great phenomenal in the orthopedic field for their bone analogue design as well as good biological and mechanical performances to satisfy specific clinical requirements. One of these biomaterials is Hydroxyapatite (HAp). HAp ($Ca_{10}(PO_4)_6(OH)_2$) a main inorganic component of bone, is an interesting biomaterial with potential for bone substitute [1], dental [2], and maxillofacial applications [3] due to its excellent biocompatibility, bioactivity, and osteoconductivity [4]. HAp, is chemically and structurally similar to the inorganic component of bone, enamel, and dentin and has received considerable attention on behalf of the biologists and biomaterial scientists [5]. It is, however, important to mention that the application of pure HAp is limited, due to its brittleness [6] while nanostructure HAp particles with a higher surface area-to-volume-ratio would be more attractive than bulk HAp particles for their application in many fields. As an example, some

34

studies demonstrated that nano-HAP particles can be used as drug carrier due to their physical and chemical properties, high surface interaction properties and their biocompatibility [7, 8]. Several studies also verified that HAp or other calcium phosphates can be used to deliver antibiotics [9], protein[10, 11], heparin and albumin adsorption [12] and anticancer and another drugs [13]. However, the tendency to aggregation of pure HAp based materials limited their further applications. Thus it is necessary to disperse such nanomaterials in suitable materials to prevent aggregation. A lot of studies [14-18] revealed that Si-substituted HAp enhanced bioactivity either in vitro or in vivo. Therefore, developing silicon-substituted hydro-xyapatite (Si-HAp) as a bioactive material was an attractive and innovative idea for enhancing bone tissue growth rate thereby improving early mechanical bone-fixation and thus leading to an enhancement in the lifetime of the implants. On the basis of these studies, Si is an essential trace element for metabolic processes associated with development of bone and connective tissues. It was reported for this case that the silica and phosphate compositions of this material are within the range that allows dissolution and calcium phosphate formation at the surface, while maintaining an appropriate rate of degradability[19, 20]. Schwarz [21] published an extensive investigation on the presence of silicon in mammalian tissues. Recently, it has been demonstrated that HAp bioactivity can be sensibly improved by the incorporation of selected ions within the apatite lattice [22]. It has been reported that, despite comparable dislocation density, Si-HAp undergo faster dissolution, occurring preferentially around grain boundaries and triple junctions [23]. Additionally,

Porter et al. confirmed that the presence of silicon inhibits grain growth helps to increased solubility and hence advanced bioactivity [17]. A variety of synthetic routes have been tried to prepare Si-HAP [14-18]. The in vitro studies suggested that Si had a critical role in the bone calcification process and the cell culture experiments during an in vitro investigation. The present study aims at the evaluation of biocompatibility effects of these materials in vitro with human osteoblasts [14, 15]. Xiao et al. [24] prepared Silicon-substituted hydroxy-apatite composite coatings on a bioactive titanium substrate by electrophoretic deposition technique with the addition of triethanolamine to enhance the ionization degree of Si-HAp suspension and were demonstrated its interaction with bovine serum albumin (BSA). Those results showed that the depositing thickness and the images of Si-HAp coating can be changed with the variation of deposition time. Moreover, it has been identified that the interaction of Ti/Si-HAp coating with BSA was much greater than that of Ti/HAp coating and suggested the incorporation of silicon in HAp was significant to improve the bioactive performance of HAp. In this study, pure nano HAp and Si substituted hydroxyapatite nanocomposites are synthesized. Morphology, surface study and size distribution of synthesized products are studied by Scanning electron microscopy (SEM) and Atomic force microscopy (AFM) respectively. Afterwards, in vitro bioactivity of these products is characterized in HSA and surface changes of these products investigated by SEM as well. Characteristic functional groups before and after soaking in HSA, are evaluated by Fourier transform infrared spectroscopy (FTIR) and in the final step, crystalline

degree of synthesized nanoproducts are also investigated by X-ray diffraction (XRD).

2. MATERIALS AND METHODS
2.1. Chemical Materials
Tetraethyl orthosilicate $(Si(OC_2H_5)_4$ (TEOS)) was purchased from Sigma–Aldrich Co. Poly (ethylene glycol) (PEG) with moderate molecular weight of 400 was used as an agent in calcium nitrate tetrahidrate $(Ca(NO_3)_2.4H_2O)$ solution to control the particle growth during precipitation. Cetylterimethil-ammonium bromide (CTAB), has been used as a moisturring agent and control growth as well, Calcium nitrate tetrahidrate $(Ca(NO_3)_2.4H_2O)$, di-ammonium hydrogen phosphate $((NH_4)_2HPO_4)$ and sodium hydroxide (NaOH), were supplied by Merck company.

2.2. Preparation of Si/Hap nanocomposites
Four Si-HAp composites with grades of Si contents (0, 2, 4 and 6 mole % as named as HS0, HS2, HS4 and HS6) were synthesized by using the following reagents: diammonium hydrogen phosphate, TEOS and calcium nitrate tetrahidrate, as precursors for P, Si and Ca source, respectively. In the first step, a 0.5 molar solution of calcium source was prepared by distilled water. Subsequently, $(NH_4)_2HPO_4$ suspension of 0.5 M was added drop wise into the prior mixture under extreme stirred for 4 h. After that, TEOS was inserted this solution and hard stirred for 24h until a good suspension was achieved. In whole process, the pH value in solution was adjusted to about 11 by using 2M solution of NaOH and the reaction temperature was kept at 25°C. The resulting solution was held unstirred for a night to remove the air bubbles trapped in viscous liquid and a good suspension achieved. Finally, the white gelatinous precipitate was separated by centrifuging (Z_36HK Hermle, Germany) the suspension at 3000 rpm for 45 min. Then the mixtures were dried in a freeze-dryer (FDE-0350, Korea) at -50°C for 48h to make powders.

2.3. In vitro bioactivity testing

HSA (human serum was obtained from the Iranian Blood Transfusion Service (Tehran, Iran)) with a concentration of 20 mg/ml was prepared to be used as simulated body fluids. Synthesized samples were immersed in HSA solutions. The solution was kept for 14 days and then dried at room temperature.

2.4. Characterization
The crystal structure and the phase present in resulting powders were analyzed with X-ray diffraction (XRD). This device (Philips PW 3710) works with voltage and current settings of 35 kV and 28.40 milliampere respectively, and uses Cu–Ka radiation (1.5405Å). For qualitative analysis, XRD diagrams were recorded in the intervals $20° \leq 2\theta \leq 45°$ at scan speed of 2°/min. The mean crystallite sizes "D" were determined according to the Scherrer equation; that is, $D = 0.9\lambda/\beta \cos \theta$, where D is the average crystallite size in A°, β is the peak broadening of the diffraction line measured at half of its maximum intensity in "radian," λ is the wavelength of X-rays, and θ is the Bragg's diffraction angle. The structures of obtained products were determined by FTIR spectrum. These products were analyzed by FTIR analysis (Perkin Elmer, USA) within scanning rang of 450-4000 cm^{-1}. The FTIR spectroscopy of this device has provided valuable information regarding the formation of HAp powder and Si/HAp products. FTIR analysis has been done to identify the

characteristic peaks of synthesized products. Scanning electron microscopy (SEM, Hitachi S-4160) was used to characterize the morphology and particle size of nanocomposites. Prior to imaging, the samples mounted on aluminum stubs were gold spattered for better conductivity. Atomic force microscopy (AFM) images showed the surface roughness, morphology and size dispersion of product obtained with a JEOL 6330F field emission device.

3. RESULTS AND DISCUSSION
3.1. XRD assessment

Figure 1 shows the XRD of the pure HAp and Si/HAp products. It seems that the silicon contents are lesser than those of the corresponding amount of starting material, containing some of silicon ions which remain in the main prior solution after precipitation. It can be specified from figures that the silicon substitution does not appear to significantly affect the diffraction pattern of hydroxyapatite. The patterns of all the samples appear to be identical, detected with no secondary phase. All the diffraction peaks on the Figure match for HAp. For whole nanoparticles samples, the existence of 2θ peaks at approximately 23.3°, 26°, 29.5°, 32°, 33° and 39°corresponding to the diffraction planes (111), (002), (210), (211), (112) and (310) of the HAp crystallites respectively, that it confirms the formation and presence of HAp in the products. It is noticeable that in the synthesis reaction of nano hydroxyapatite, β-tri calcium phosphate (β-TCP) can be fabricated. It is resulted

in broadening of HAp peaks due to HAp and β-TCP peaks overlapping. It can be seen that crystalline structure refers in prepared products by in situ hybridization method. As it was shown in Figure 1 the crystalline characteristic peaks of HAp were not alteration significantly, it is also noted that peaks in the precipitated Si/HAp nano-composites became broader and weaker slightly as compared to the pure HAp nanoparticles, which could be resulted from the interface binding between particles simultaneously. These reflections could not be broader and less intense as the TEOS content increases. However, these patterns do not reveal the presence of extra phases. It seems that Silicon substitution were did not have any effect on the diffraction pattern of hydroxyapatite. The small changes in the crystal structure derived from incorporation of a slightly larger silicate ion in the location of phosphate ions and accrue to loss of some of the OH groups in the composites. It could be due to the molecular interactions between HAp and Si content. As it is shown in these figures, by increasing of TEOS content, the crystalline size of composite samples slightly decreased which is also confirmed by the micrograph results. Finally, with respect to the crystalline size of the products in XRD, the peak at $2\theta = 23.5°$ were chosen. Crystallite size was calculated using Scherer's equation, the report shows that the approximate crystallite sizes of HS0, HS2, HS4, and HS6 samples were 47, 40, 23 and 12 nm.
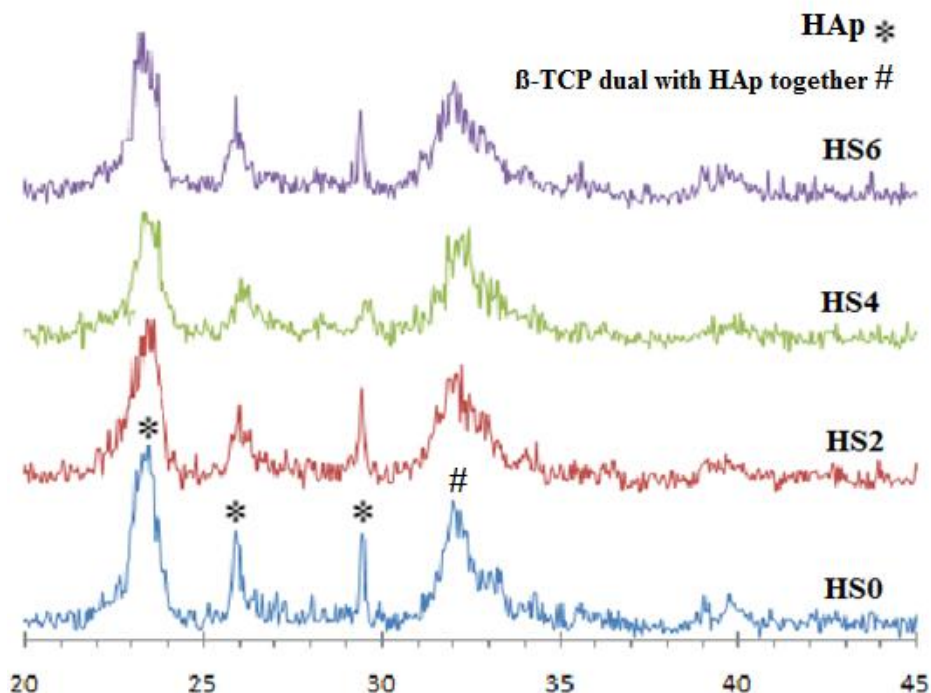
Figure 1. XRD pictures of the samples before soaking in HSA

3.2. FT-IR investigation

FTIR was used to study the synthesized composites to characterize the effect of the silicon substitution on the different functional groups. Figure 2 shows the FT-IR spectra of the synthesized HAp and Si/HAp samples. The spectra of the synthesized materials were found to be quite similar. The bands at 1480, and 1380 cm-1 correspond to carbonate band in whole samples. The intense bands at 1100, 1030, and 965 cm^{-1} are compared, which correspond to P–O stretching vibration modes, as well as the bands at 604 and 566 cm-1 correspond to the O–P–O bending mode. The peak at 1630 cm^{-1} attributes to the bending vibration of O–H of water absorbed in the sample. The relative width intensity of the OH bands and PO_4^{3-} bands were slightly reduced in Si/HAp samples for synthesized powders that might be due

to interaction between Si and HAp. More significantly, new band appearing at 880 cm^{-1} for Si/HAp samples was assigned to Si–O vibration modes of SiO_4^{4-} groups. Additionally, another new band appearing at 820 cm^{-1} for Si/HAp samples was assigned to Si–O–Si vibration modes of SiO_4^{4-} groups which were polymerized. The FT-IR analysis comparison confirmed that the significant existence of HAp nanoparticles surrounded at nanocomposites for different samples and this spectrum showed absorption bands of Carbonated-Hydroxyapatite. Finally, the broad band around at 3500 cm^{-1}, as well as the band corresponds to moisture or OH group of water in the whole samples. The observation of the spectra as a function of the TEOS content shows the bands corresponding to OH groups and PO_4^{3-} groups. The width of peaks decrease as the TEOS

contents increases. In contrast, the bands corresponding to CO_3^{2-} groups increase with the TEOS content. This interesting point was seen after composites composed, the OH broad band in composite samples became weaker and decreased, which can be due to the reduction of water adsorption after formation of the composites.
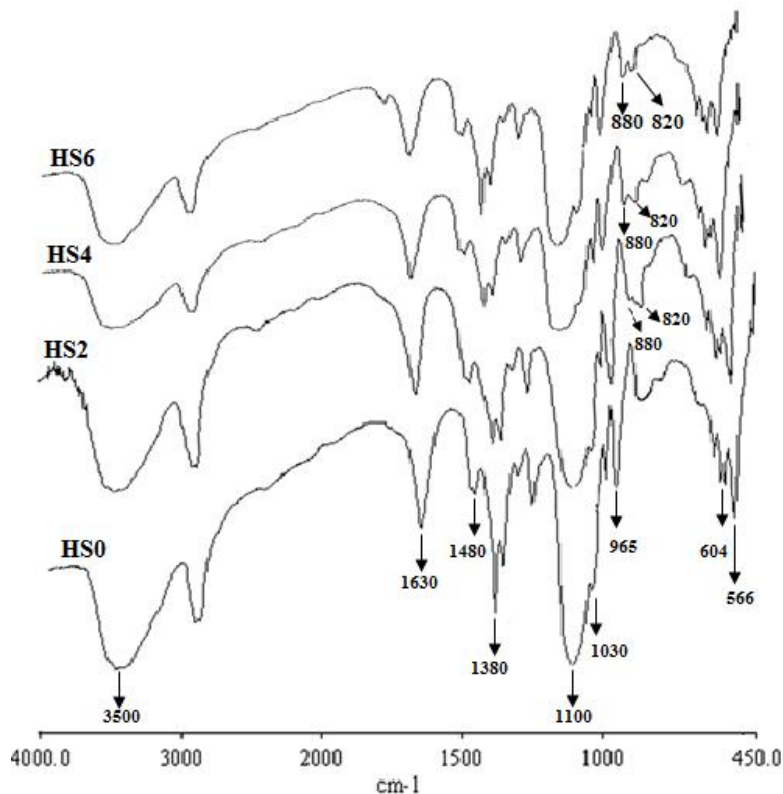

Figure 2. FTIR spectra of the samples before soaking in HSA

3.3 SEM and AFM analysis

Figure 3. a, b, c and d indicates the SEM micrographs of the HS0, HS2, HS4 and HS6 with different contents of Si respectively. Many particle aggregations were found in the composite products that according to micrographs, increasing in amounts of loaded Si the distribution and agglomeration of particles on surface of the composites were significantly changed. However, many small particle crystallites existed in the aggregated surface was observed. The improvement of surface modification in these products might be due to high solubility of the nanoparticles in the organic solvents that it prevented further augment particles agglomeration on the surfaces. Figure 4 (a–d) was used to determine surface topography and illustrated the surface properties of the synthesized products in 3D and 2D topographies by AFM. In this Figure (b, c, d), Si/HAp samples presented different morphology as compared to pure HAp that it exhibited dispersed nanoparticles in the solution. As it can be seen, composite samples had a relatively smooth and uniform surface rather than HS0. This appeared increasing of various Si content could modify and improved the surface of pure HAp; similarity give the impression resulted in SEM and confirmed these outcomes. This figure

indicated the Si particles had a core effect on the polymerization of composites formation. It looked penetration of Si particles into the prior solution led to similar formations of aggregates and agglomerates on the surface of composites. On the other hand, existence of these particles negligibly increased surface roughness in the composites. The micrograph illustrates the presence of agglomerations among the particles, which can be resulted from the interface binding between produced samples, that can be due to high specific surface energy of nanoparticles resulting in their aggregations. These interesting results are evidence, these particles could also control the particles in composite as depicted in the SEM micrograph and we can see the most present of aggregation occurred on the nanocomposites surface as well. This is noticeable that the Si particles in triple nanocomposites have been covered with a continuous smooth layer and the particle sizes of composites are almost smaller due to the increasing values of Si. However, by observing in the resulted micrograph the TEOS content had a negative effect on the crystal size and the mean value of crystal size decreased with the increase of TEOS content. The AFM and SEM pictures gave an idea about the pure HAp is crystallite stick-shaped, however, more needle-shaped crystallites increased with the TEOS content in composites, pointing out that the growing of composite products to be easier in the presence of TEOS but it needs more investigation.
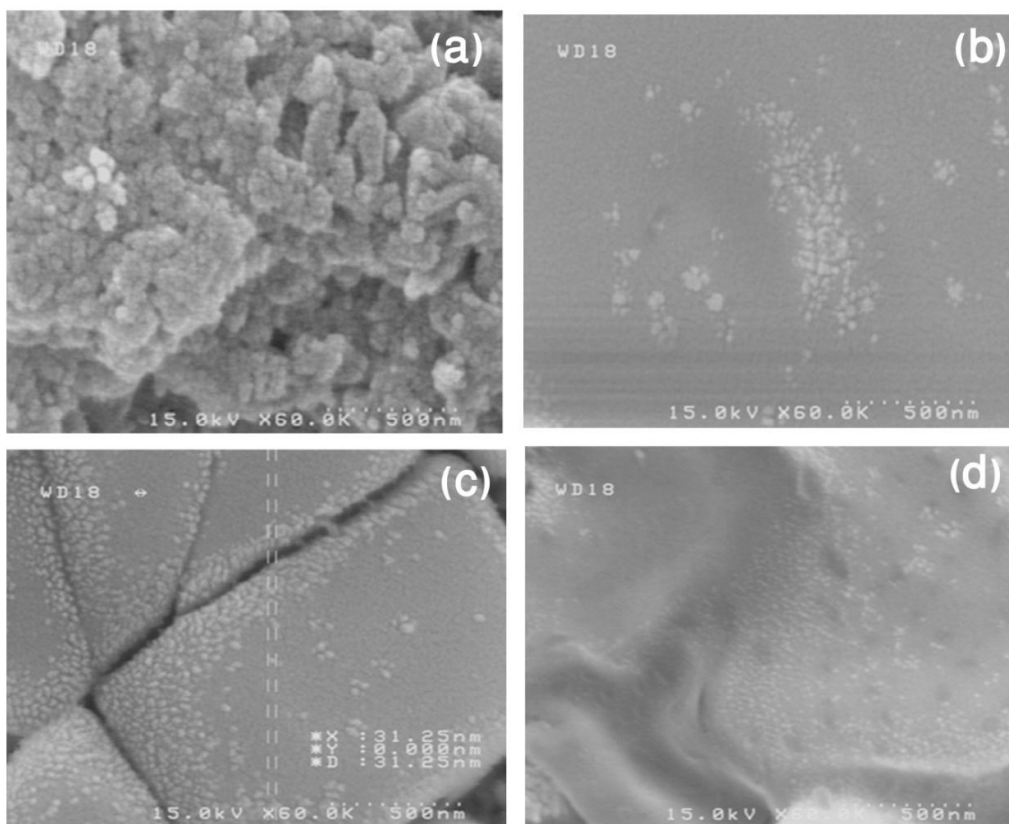

Figure 3. SEM micrographs of (a) HS0, (b) HS2, (c) HS4 and (d) HS6 before soaking in HSA
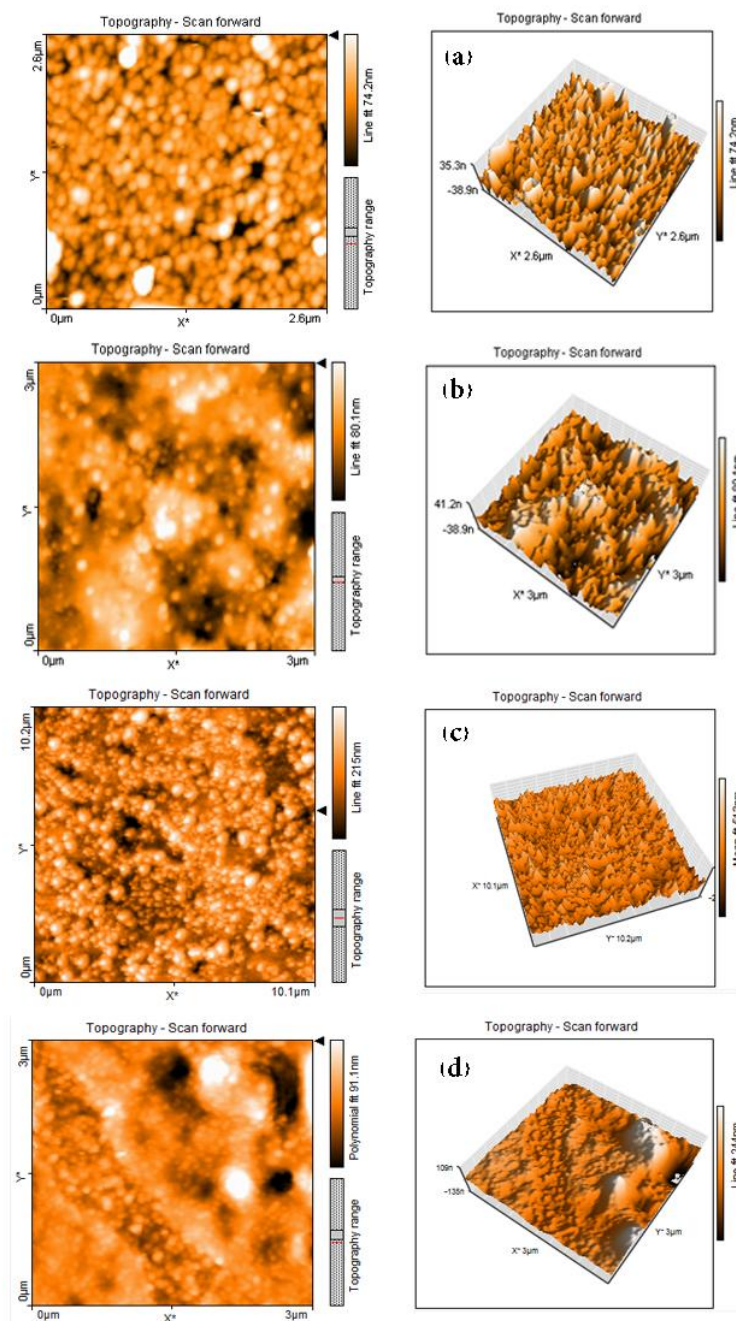
Figure 4. AFM images of (a) HS0, (b) HS2, (c) HS4 and (d) HS6

3. 4 Size distribution of products by AFM results

Figure 5 shows particles size distribution of the products, which demonstrates the HS0 particles size were between 5 and 255 nm with further mean size of approximately 65 nm, while size distribution for the composite samples were in the range of less than 211, 164 and 86 nm, respectively, and most of the tiniest particles were found to be 54, 50 and

21 nm for HS2, HS4 and HS6 respectively. These outcomes confirmed the results of SEM and XRD. In other word, it indicated that increasing in various contents of Si decreases particle size of composites and size distribution of samples become better than the pure HAp.
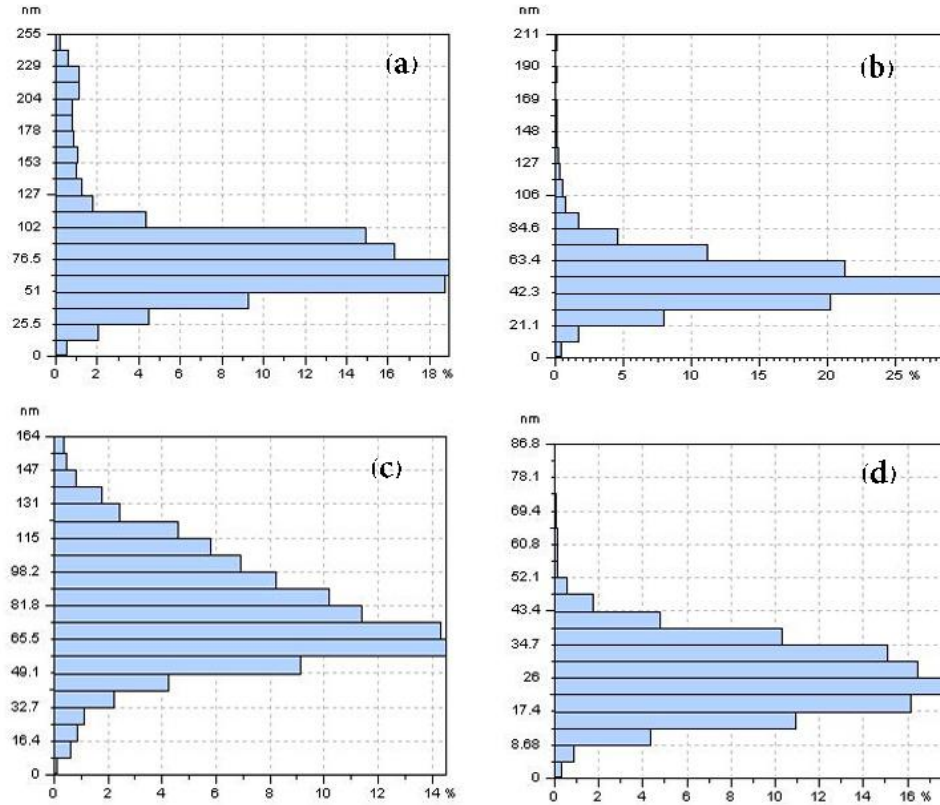

Figure 5. Size distribution of (a) HS0, (b) HS2, (c) HS4 and (d) HS6

3.5 In vitro assessment

In order to evaluate the samples bioactivity, the synthesized nanocomposites were soaked in HSA solution. Figure 6 shows SEM images (using VEGAII TESCAN instrument) of the Si/HAp samples after immersion in HSA for periods of 14 days. After soaking, the morphology of the particles partially became obscure accordingly; soaking caused tiny particles to be seen in a new formation, as the new form of apatite layer covered these same as observable. The surfaces of the long time soaked samples was covered with these apatite layers that were confirmed using FTIR figures after immersion that is shown in Figure 7. Comparing these figures indicates the new obtained pattern after soaking specified apatite, and this high low intensity can distinguish the new formed apatite from the original Si/HAp due to the low crystallinity of new formed apatite. Soaking in HSA led to formation of an apatite layer on the surface of the samples which can be seen in the SEM results. From the

FTIR result in Figure 7, it is quite obvious that all of the peaks in FTIR remained after soaking, but peaks intensity was decreased and compressed although the intensity of phosphate and carbonate groups peaks increased in comparison with the other peaks. This is because of the soaking effect in HSA solution and the slight shift to the right turned to be the result of HSA and other samples interaction. On the samples there are many nano particles which could act as nucleation sites. It is noticeable that the OH broad peak eliminated after soaking, that this loss of OH groups might be due to the incorporation of silicon in to HAp structure with silicate-substituted hydroxyapatite being formed. It may also be due to the formation of Hydroxyapatite or good interaction between HSA and the samples. It appeared in the same interval of time; more apatite was deposited on the composites other than on the HAp alone that is difficult to study by SEM figures and needs more investigation. Consequently, each particle formed on the composites was smaller than the HAp. It is suggested that the major reason of apatite formation enhancement on the composites might be the n-HAp particles acted as nucleation initiation sites. The formation of apatite was observed on the pure HAp surface as well as into the matrix of composites. These formed apatite crystals are in dense form and organized as homogeneously covering the surface after 14 days of mineralization. The SEM figure after immersion determined that the surface was covered with a uniform mineral coating that it maybe formed calcium phosphate in the apatite structure. Moreover, these figures showed in some regions of the composites, the apatite crystals were present in the form of clusters of needles that they were expected to be in the nanometer range. It seems to be difficult to show, based on these results through FTIR, a new form of apatite formed after soaking in HSA which needs more analysis. Figures 3 and 7 showed surface difference of the samples before and after soaking in HSA by SEM. In all of the samples it can be seen the apatite particles which formed on the surface after soaking in HSA. It can be concluded from the images that larger amount of HAp in the content of the samples led to formation of smaller apatite particles on the surface. However, it needs further investigation.
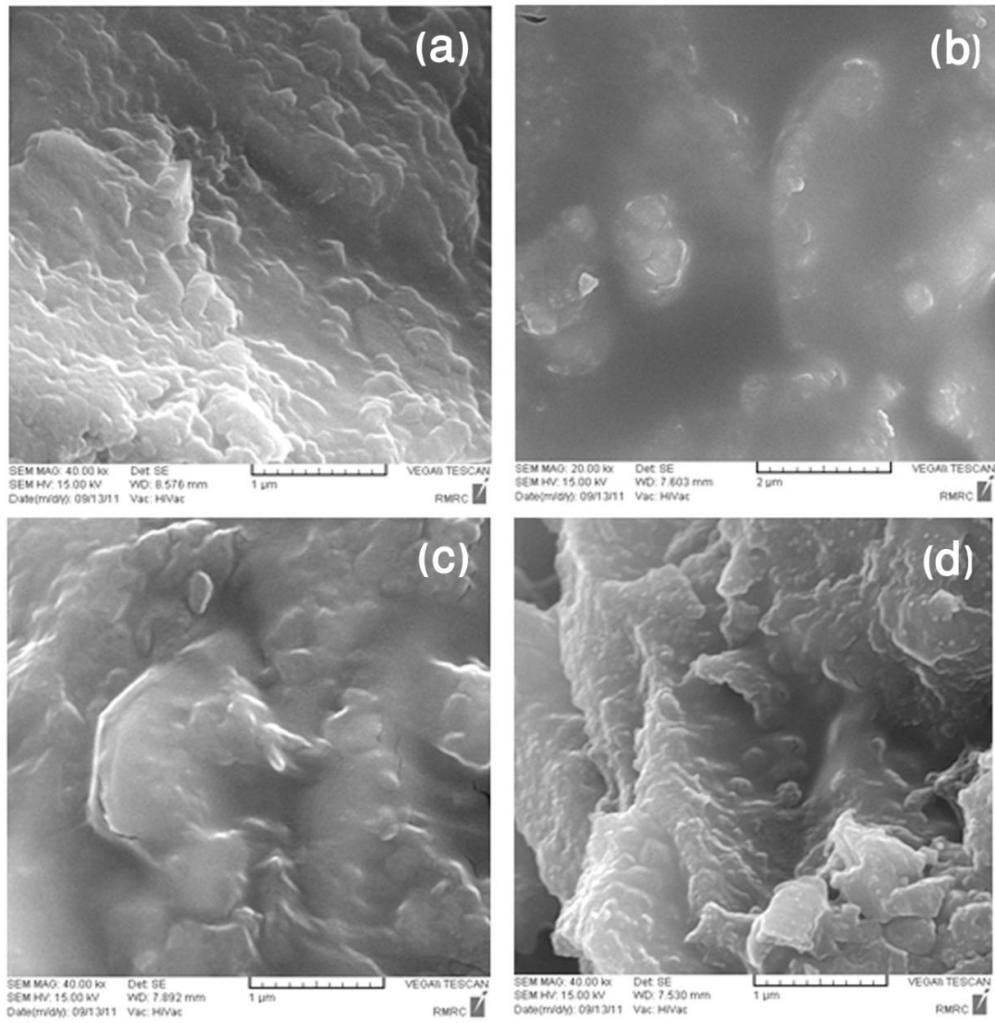
Figure 6. SEM micrographs of (a) HS0, (b) HS2, (c) HS4 and (d) HS6 after soaking in HSA
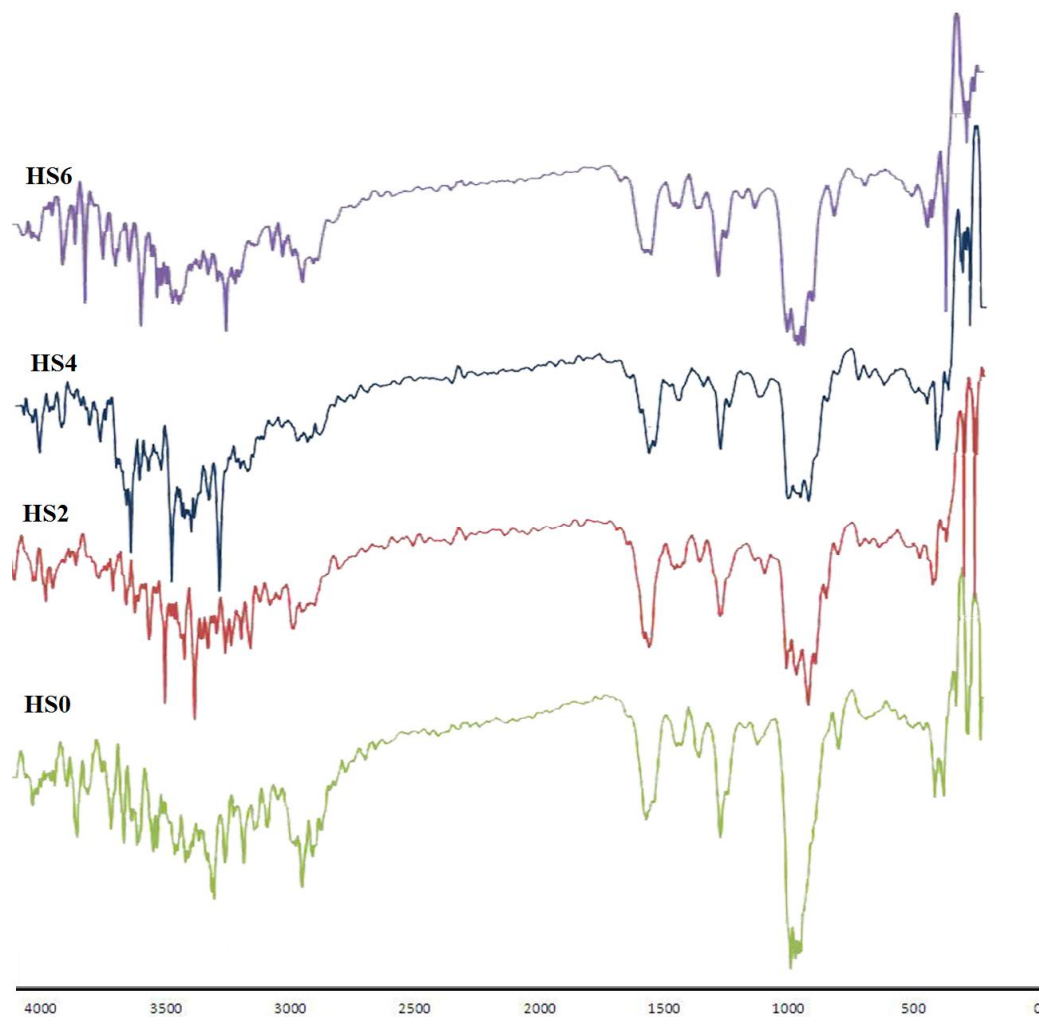
HS6

HS4

HS2

HS0

| 4000 | 3500 | 3000 | 2500 | 2000 | 1500 | 1000 | 500 | 0 |

Figure 7. FTIR spectra of the sample after soaking in HSA

4. CONCLUSION

Nano Hydroxyapatite and Silicon-substituted hydroxyapatite nano-composites were prepared by in situ hybridization method using $(NH_4)_2HPO_4$, Ca $(NO_3)_2.4H_2O$, TEOS and PEG as a reagent. The effects of silicon-substituted hydroxyapatite materials towards the responses of HSA were investigated and compared to the pure hydroxyapatite responses and proved interesting information after these soaking. SEM and AFM results in this paper (herein) indicated by increasing of various content of Si, particle size of composites decreased and size distribution of samples were better than the pure HAp. In addition, there were many tiny particle structures that existed on the surface of the composites thus as to these scales were in nanometers which makes the surface, arrange in order, that used from 2d and 3d AFM pictures for confirming of these results. These outcomes suggested ordering of crystals could improve in the contact of protein and these might be able to cause of Si-HAp with high quality dissolve in the HSA solution. Deduced this superior interaction between protein and Synthesized nano products,

the biomineralization process of Si-HAp samples and the highly self-assembly structure forms of these, would make the biomineralization of samples possess the same chemical components with bone tissues that must be investigated by in vivo test. Therefore, it is proposed that the synthesized nanomaterial maybe can better support new bone tissue regeneration at the site of implantation and maintain sufficient integrity for bone substitute. These results recommend that the interaction of synthesized nanocomposite samples with HSA were greatly better than the HS0 which could be cause of the great incorporation of small amount of silicon in the HAp. In addition, this high-quality incorporation excellently improved the reactive performance of all the synthesized samples with HSA, that appears due to use of in situ hybridization method.

REFERENCES

[1] A. Sionkowska, J. Kozłowska, *Int. J. Biol. Macromol.* 47, 483 (**2010**).

[2] M. Sadat-Shojai, M. Atai, A. Nodehi, L.N. Khanlar, *Dent. Mater.* 26, 471 (**2010**).

[3] F.Z. Notodihardjo, N. Kakudo, S. Kushida, K. Suzuki, K. Kusumoto, *J. Craniomaxillofac. Surg.* 40, 287 (**2012**).

[4] F. Tan, M. Naciri, D. Dowling, M. Al-Rubeai, *Biotechnol. Adv.* 30, 352 (**2012**).

[5] L. Fang, Y. Leng, P. Gao, *Biomaterials* 26, 3471 (**2005**).

[6] H. Zhou, J. Lee, *Acta Biomater.* 7, 2769 (**2011**).

[7] K. Sugo, T. Yoshitake, M. Tomita, S. Kobayashi, Y. Kurosawa, K. Kawamura, T. Okuyama, *Sep. Purif. Technol.* 76, 432 (**2011**).

[8] K. Tomoda, H. Ariizumi, T. Nakaji, K. Makino, *Colloids Surf. B. Biointerfaces* 76, 226 (**2010**).

[9] S. Leprêtre, F. Chai, J.-C. Hornez, G. Vermet, C. Neut, M. Descamps, H.F. Hildebrand, B. Martel, *Biomaterials* 30, 6086 (**2009**).

[10] S. Ishihara, T. Matsumoto, T. Onoki, M.H. Uddin, T. Sohmura, A. Nakahira, *Acta Biomater.* 6, 830 (**2010**).

[11] A. Talal, N. Waheed, M. Al-Masri, I. McKay, K. Tanner, F. Hughes, *J. Dent.* 37, 820 (**2009**).

[12] S.P. Victor, C.P. Sharma, *Colloids Surf. B. Biointerfaces* 85, 221 (**2011**).

[13] S.P. Pathi, D.D. Lin, J.R. Dorvee, L.A. Estroff, C. Fischbach, *Biomaterials* 32, 5112 (**2011**).

[14] E. Thian, J. Huang, S. Best, Z. Barber, W. Bonfield, *J. Mater. Sci. Mater. Med.* 16, 411 (**2005**).

[15] E. Thian, J. Huang, S. Best, Z. Barber, W. Bonfield, *Biomaterials* 26, 2947 (**2005**).

[16] N. Patel, S. Best, W. Bonfield, I. Gibson, K. Hing, E. Damien, P. Revell, *J. Mater. Sci. Mater. Med.* 13, 1199 (**2002**).

[17] A. Porter, N. Patel, J. Skepper, S. Best, W. Bonfield, *Biomaterials* 24, 4609 (**2003**).

[18] N. Hijón, M.V. Cabanas, J. Pena, M. Vallet-Regí, *Acta Biomater.* 2, 567 (**2006**).

[19] D. Arcos, M. Vallet-Regí, *Acta Biomater.* 6, 2874 (**2010**).

[20] S. Rabiee, S. Mortazavi, F. Moztarzadeh, D. Sharifi, S. Sharifi, M. Solati-Hashjin, H. Salimi-Kenari, D. Bizari, *Biotechnol. Bioprocess Eng.* 13, 204 (**2008**).

[21] K. Schwarz, *Proceedings of the National Academy of Sciences* 70, 1608 (**1973**).

[22] I.R. Gibson, S.M. Best, W. Bonfield, *J. Am. Ceram. Soc.* 85, 2771 (**2002**).

[23] C. Botelho, M. Lopes, I. Gibson, S. Best, J. Santos, *J. Mater. Sci. Mater. Med.* 13, 1123 (**2002**).

[24] F.-J. Xiao, Y. Zhang, L.-J. Yun, *Trans. Nonferrous Met. Soc. China* 19, 125 (**2009**).